Journal of Sound and Vibration (2000) **235**(1), 87–104
doi:10.1006/jsvi.2000.2909, available online at http://www.idealibrary.com on IDEAL®

COMPARATIVE STUDIES ON MOVING FORCE IDENTIFICATION FROM BRIDGE STRAINS IN LABORATORY

TOMMY H. T. CHAN, LING YU AND S. S. LAW

Department of Civil and Structural Engineering, The Hong Kong Polytechnic University, Hung Hom, Kowloon, Hong Kong. E-mail: cetommy@polyu.edu.uk

(*Received* 30 *August* 1999, *and in final form* 12 *February* 2000)

Force identification from dynamic responses of bridges is an important inverse problem. The parameters of both the vehicle and the bridge play an important role in the force identification. Based on the bending moments measured in the laboratory and the four identification methods developed, this paper aims to investigate the effect of various parameters on the four methods. For this purpose, a bridge–vehicle system model has been designed in the laboratory. The bending moments and acceleration responses of the model bridge are simultaneously measured when the model vehicle moves across the bridge at different speeds. The moving forces are identified from the bridge strains using the four methods, and the rebuilt responses are calculated from the identified forces for comparative studies on the four methods. Assessment results show that all four methods are effective and acceptable with higher accuracy to some extent. The TDM is the best and is strongly recommended for incorporation into a moving force identification system (MFIS).

1. INTRODUCTION

Many methods have been presented for force identification in recent years [1–8]. Stevens [9] has given an excellent survey of the literature on the force identification problem as well as an overview. However, most of the methods mentioned measure only static axle loads. O'Connor and Chan [10] suggested an advanced force identification method — Interpretive Method I (IMI) to interpret the force history, which is an advancement of the weight-in-motion methods mentioned above and is able to measure the dynamic axle forces of multi-axle systems. Based on system identification theory, the authors have developed another two moving force identification methods, namely the time-domain method (TDM) [11] and the frequency–time-domain method (FTDM) [12]. Recently, a new method similar to IMI, the Interpretive Method II (IMII), has also been published [13]. Preliminary studies [14] showed that all these four methods could identify moving forces with acceptable accuracy. However, each method has its merits, limitations and disadvantages. They need to be improved and enhanced for practical application in field tests. It is also a good idea to merge them into a moving force identification system (MFIS). Therefore, comparative studies on the four methods based on the measured bending moments are described in this paper. The effects of various parameters on the force identification have been critically investigated using experimental data. The parameters include the bridge mode numbers used, sampling frequencies, vehicle speeds, computational time, sensor numbers and locations. Acceptable results on identified forces are obtained and some suggestions are made for the identification methods.

0022-460X/00/310087 + 18 $35.00/0

2. DESCRIPTION OF IDENTIFICATION METHODS

2.1. ANALYTICAL MODELS

The moving force identification described here is an inverse of a forward problem, whereby structural responses caused by a set of time-varying forces running across a bridge are found. In the inverse problem, forces are deduced from measured responses instead. Two models can be used for this kind of analysis.

2.1.1. *Beam-element-model*

A simply supported bridge can be modelled as an assembly of lumped masses interconnected by massless elastic beam elements as shown in Figure 1, and the nodal responses for displacements or/and bending moment at any instant are given by equations (1) and (2) respectively,

$$\{Y\} = [Y_A]\{P\} - [Y_I][\Delta m]\{\ddot{Y}\} - [Y_I][C]\{\dot{Y}\}, \tag{1}$$

$$\{M\} = [M_A]\{P\} - [M_I][\Delta m]\{\ddot{Y}\} - [M_I][C]\{\dot{Y}\}, \tag{2}$$

where $\{P\}$ is the vector of wheel loads, $[\Delta m]$ is the diagonal matrix containing values of lumped mass, $[C]$ is the damping matrix, $\{M\}$, $\{Y\}$, $\{\dot{Y}\}$, $\{\ddot{Y}\}$ are the nodal bending moment, displacement, velocity, acceleration vectors respectively, $[Y_A]$, $[Y_I]$ are matrices for nodal forces to obtain nodal displacements, and $[M_A]$, $[M_I]$ are matrices for nodal forces to obtain nodal bending moments.

2.1.2. *Continuous beam model*

The bridge model is considered as a simply supported beam with a span length L, constant flexural stiffness EI, constant mass per unit length ρ and viscous proportional damping C. The effects of shear deformation and rotary inertia are not taken into account (Bernoulli–Euler beam). If the force P moves from left to right at a speed c, as shown in Figure 2, then an equation of motion can be expressed as

$$\rho \frac{\partial^2 v(x,t)}{\partial t^2} + C \frac{\partial v(x,t)}{\partial t} + EI \frac{\partial^4 v(x,t)}{\partial x^4} = \delta(x - ct)P(t), \tag{3}$$

where $v(x, t)$ is the beam deflection at point x and time t and $\delta(x - ct)$ is the Dirac delta function. Based on modal superposition, if the nth mode shape function of the beam $\Phi_n(x) = \sin(n\pi x/L)$, the solution of equation (3) can be expressed as follows:

$$v(x,t) = \sum_{n=1}^{\infty} \sin \frac{n\pi x}{L} q_n(t), \tag{4}$$

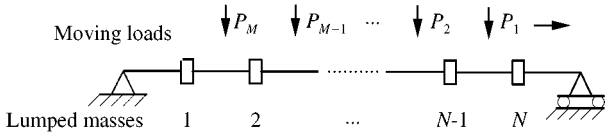

Figure 1. Beam-element model.

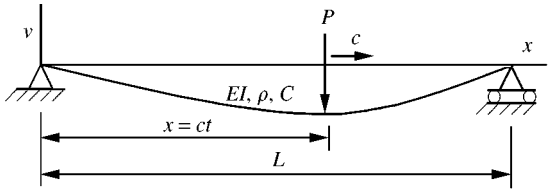

Figure 2. Moving force on a simple supported beam.

where n is the mode number, and $q_n(t)$ ($n = 1, 2, \ldots, \infty$) are the nth modal displacements. After substituting equation (4) into equation (3), integrating the resultant equation with respect to x between 0 and L, and then using the boundary conditions and the properties of the Dirac delta function, the equation of motion in terms of the modal displacement $q_n(t)$ can be expressed as

$$\ddot{q}_n(t) + 2\xi_n\omega_n\dot{q}(t) + \omega_n^2 q_n(t) = \frac{2}{\rho L}\, p_n(t) \quad (n = 1, 2, \ldots, \infty), \tag{5}$$

where

$$\omega_n = \frac{n^2\pi^2}{L^2}\sqrt{\frac{EI}{\rho}}, \quad \xi_n = \frac{C}{2\rho\omega_n}, \quad p_n(t) = P(t)\sin\left(\frac{n\pi\bar{x}}{L}\right) \tag{6}$$

are the nth modal frequency, the modal damping and the modal force respectively. $\bar{x}$ is the distance of the axle from the left-hand support. If the time-varying force $P(t)$ is known, equation (5) can be solved to yield $q_n(t)$ and the dynamic deflection $v(x, t)$ can then be obtained form equation (4). This is called the forward problem. The moving force identification is an inverse problem, in which the unknown time-varying force $P(t)$ is identified using the measured displacements, accelerations or bending moments of real structures. Three methods are developed for the purpose. The IMII is developed directly using the continuous beam model, the TDM and FTDM are developed using the continuous beam model associated with the system identification concept.

2.2. MOVING FORCE IDENTIFICATION METHODS

2.2.1. *Interpretive Method I* (**IMI**)

This method is developed using the beam-element model. As stated in Section 2.1.1, solutions can be developed using the $\ddot{Y}$ (accelerations), Y (displacements) or M (bending moments). If Y is known at all times for all interior nodes, $\dot{Y}$ and $\ddot{Y}$ can be obtained using numerical differentiation. Equation (1) then becomes an over-determined set of linear simultaneous equations in which P can be solved. Similarly, if $\ddot{Y}$ is known, it can be integrated by an integration method to give $\dot{Y}$ and Y, further to get P. However, a particular difficulty arises if measured bending moments are used as input data. Remembering that the moving load P is not always at the nodes, and the relation between the nodal displacements and the nodal bending moments is

$$\{Y\} = [Y_B]\{M\} + [Y_C]\{P\} \tag{7}$$

where $[Y_C]\{P\}$ allows for the deflections due to an additional triangularly distributed bending moments that occur within elements carrying one or more point loads P. $[Y_C]$ can be calculated from the known locations of the loads. Both $[Y_B]$ and $\{M\}$ are known, but $\{Y\}$ cannot be determined without a knowledge of $\{P\}$. O'Connor and Chan described a solution in detail in reference [10].

2.2.2. *Interpretive Method II* (**IMII**)

If there are k moving loads on the beam, equation (5) can be written as

$$\begin{Bmatrix} \ddot{q}_1 \\ \ddot{q}_2 \\ \vdots \\ \ddot{q}_n \end{Bmatrix} + \begin{Bmatrix} 2\xi_1\omega_1\dot{q}_1 \\ 2\xi_2\omega_2\dot{q}_2 \\ \vdots \\ 2\xi_n\omega_n\dot{q}_n \end{Bmatrix} + \begin{Bmatrix} \omega_1^2 q_1 \\ \omega_2^2 q_2 \\ \vdots \\ \omega_n^2 q_n \end{Bmatrix}$$

$$= \frac{2}{\rho L} \begin{bmatrix} \sin\dfrac{\pi(ct-\hat{x}_1)}{L} & \sin\dfrac{\pi(ct-\hat{x}_2)}{L} & \cdots & \sin\dfrac{\pi(ct-\hat{x}_k)}{L} \\ \sin\dfrac{2\pi(ct-\hat{x}_1)}{L} & \sin\dfrac{2\pi(ct-\hat{x}_2)}{L} & \cdots & \sin\dfrac{2\pi(ct-\hat{x}_k)}{L} \\ \vdots & \vdots & \vdots & \vdots \\ \sin\dfrac{n\pi(ct-\hat{x}_1)}{L} & \sin\dfrac{n\pi(ct-\hat{x}_2)}{L} & \cdots & \sin\dfrac{n\pi(ct-\hat{x}_k)}{L} \end{bmatrix} \begin{Bmatrix} P_1 \\ P_2 \\ \vdots \\ P_k \end{Bmatrix} \tag{8}$$

in which $\hat{x}_k$ is the distance between the kth load and the first load, and $\hat{x}_1 = 0$. Therefore, as mentioned above, the modal displacements at $x_1, x_2, \ldots, x_l$ can be obtained by solving equation (8) and the displacements at $x_1, x_2, \ldots, x_l$ can also be obtained from the second derivative of the displacements, and the bending moments at the corresponding locations can be obtained from the relationship $M = -EI(\partial^2 v/\partial x^2)$.

If $P_1, P_2, \ldots, P_k$ are known constant moving loads and the effect of damping is ignored, the closed-form solution of equation (3) is given as

$$v(x,t) = \frac{L^3}{48EI} \sum_{i=1}^{k} P_i \sum_{n=1}^{\infty} \frac{1}{n^2(n^2-\alpha^2)} \sin\frac{n\pi x}{L} \left(\sin\frac{n\pi(ct-\hat{x}_i)}{L} - \frac{\alpha}{n} \sin\omega_n\left(t - \frac{\hat{x}_i}{c}\right)\right) \tag{9}$$

in which $\alpha = \pi c/L\omega_n$. Therefore, if the displacements of the beam at $x_1, x_2, \ldots, x_l$ caused by a set of constant moving force loads are known, the magnitude of each moving load can be obtained by solving the following equation:

$$\{v\} = [S_{vP}]\{P\} \tag{10}$$

or

$$\begin{Bmatrix} v_1 \\ \vdots \\ v_m \\ \vdots \\ v_l \end{Bmatrix} = \begin{bmatrix} s_{11} & \cdots & s_{1i} & \cdots & s_{1k} \\ \vdots & \ddots & & & \vdots \\ s_{m1} & & s_{mi} & & s_{mk} \\ \vdots & & & \ddots & \vdots \\ s_{l1} & \cdots & s_{li} & \cdots & s_{lk} \end{bmatrix} \begin{Bmatrix} P_1 \\ \vdots \\ P_i \\ \vdots \\ P_k \end{Bmatrix}, \tag{11}$$

where

$$s_{mi} = \frac{L^3}{48EI} \sum_{n=1}^{\infty} \frac{1}{n^2(n^2 - \alpha^2)} \sin \frac{n\pi x_m}{L} \left(\sin \frac{n\pi(ct - \hat{x}_i)}{L} - \frac{\alpha}{n} \sin \omega_n \left(t - \frac{\hat{x}_i}{c} \right) \right). \tag{12}$$

If $l \geqslant k$, which means that the number of displacement measuring stations is larger than or equal to the number of axle loads, $\{P\}$ can be obtained using the least-squares estimate

$$\{P\} = ([S_{vP}]^{\mathrm{T}}[S_{vP}])^{-1}[S_{vP}]^{\mathrm{T}}\{v\}. \tag{13}$$

A similar equation can be obtained using bending moments instead of displacements by considering the closed-form solution in terms of bending moments.

2.2.3. *Time-domain method* (**TDM**)

Equation (5) can be solved in the time domain by the convolution integral and the dynamic deflection $v(x, t)$ of the beam at point x and time t can be obtained as

$$v(x, t) = \sum_{n=1}^{\infty} \frac{2}{\rho L \omega_n'} \sin \frac{n\pi ct}{L} \int_0^t \mathrm{e}^{-\xi_n \omega_n (t-\tau)} \sin \omega_n'(t - \tau) \sin \frac{n\pi c\tau}{L} P(\tau)\, \mathrm{d}\tau, \tag{14}$$

where $\omega_n' = \omega_n \sqrt{1 - \xi_n^2}$. Therefore, the bending moment in the beam at point x and time t is

$$m(x, t) = -EI \frac{\partial^2 v(x, t)}{\partial x^2} = \sum_{n=1}^{\infty} \frac{2EI\pi^2 n^2}{\rho L^3 \omega_n'} \sin \frac{n\pi ct}{L} \int_0^t \mathrm{e}^{-\xi_n \omega_n (t-\tau)} \sin \omega_n'(t - \tau) \sin \frac{n\pi c\tau}{L} P(\tau)\, \mathrm{d}\tau. \tag{15}$$

The acceleration at point x and time t is

$$a(x, t) = \ddot{v}(x, t) = \sum_{n=1}^{\infty} \frac{2}{\rho L} \Phi_n(x) \left[P(t) \sin \left(\frac{n\pi ct}{L} \right) + \int_0^t \ddot{h}^n(t - \tau) P(\tau) \sin \left(\frac{n\pi c\tau}{L} \right) \mathrm{d}\tau \right], \tag{16}$$

where

$$\ddot{h}_n(t) = \frac{1}{\omega_n'} \mathrm{e}^{-\xi_n \omega_n t} \{ [(\xi_n \omega_n)^2 - \omega_n'^2] \sin \omega_n' t + [-2\xi_n \omega_n \omega_n'] \cos \omega_n' t \}. \tag{17}$$

Assume that both the time-varying force $P(t)$ and the bending moment $m(x, t)$ or the acceleration $a(x, t)$ are step functions in a small time interval Δt; equations (15) and (16) can be rewritten in discrete terms and rearranged into a set of equations as follows:

$$\mathbf{B}_{\mathrm{N} \times \mathrm{N_B}} \mathbf{P}_{\mathrm{N_B} \times 1} = \mathbf{R}_{\mathrm{N} \times 1} \tag{18}$$

where $\mathbf{P}$ is the time-series vector of the time-varying force $P(t)$, $\mathbf{R}$ is the time-series vector of the measured response of the bridge deck at the point x, such as the bending moment $m(x, t)$ or acceleration $a(x, t)$. The system matrix $\mathbf{B}$ is associated with the system of the bridge deck

and the force. The subscripts $\mathbf{N_B} = L/c\Delta t$ and $\mathbf{N}$ are the numbers of sample points for the force $P(t)$ and measured response $\mathbf{R}$ respectively when the force moves across the whole bridge deck.

2.2.4. *Frequency-time domain method* (**FTDM**)

Equation (5) can also be solved in the frequency domain. Performing the Fourier transform for equation (5) and $v(\mathrm{x}, t) \sum_{n=1}^{\infty} \Phi_n(x) q_n(t)$, the Fourier transform of the dynamic deflection $v(x, t)$ is

$$V(x, \omega) = \sum_{n=1}^{\infty} \frac{2}{\rho L} \Phi_n(x) H_n(\omega) P(\omega), \tag{19}$$

where $H_n(\omega)$ and $P(\omega)$ are the Fourier transforms of $q_n(t)$ and $P(t)$ respectively. Similarly, the relationships between bending moment or acceleration and dynamic deflection can also be used to execute the corresponding Fourier transform. Finally, a set of N-order simultaneous equations can be established in the frequency domain. The force $P(\omega)$ consisting of the real and imaginary parts can be found by solving the Nth order linear equations. The time history of the time-varying force $P(t)$ can then be obtained by performing the inverse Fourier transformation. From the procedures mentioned above, the governing equations are initially formulated in the frequency domain. However, the solution is obtained in the time domain, and this method is therefore called frequency–time-domain method.

The above procedure is derived for the identification of a single force using the TDM and FTDM. They can be modified for the identification of multi-forces using the linear superposition principle.

3. EXPERIMENTAL DESIGN IN LABORATORY

The model car and model bridge deck were constructed in the laboratory. An axle spacing to span ratio (ASSR) is defined as the ratio of the axle spacing between two consecutive axles of the vehicle to the bridge span length. Here, the ASSR was set to be 0·15. The model car had two axles at a spacing of 0·55 m and was mounted on four rubber wheels. The static mass of the whole vehicle was 12·1 kg in which the mass of rear wheel was 3·825 kg. The model bridge deck consisted of a main beam, a leading beam and a trailing beam as shown in Figure 3. On the leading beam a constant vehicle speed was reached as the model car approached the bridge. The trailing beam was used for decelerating the car. The main beam with a span of 3·678 m long and 101 mm × 25 mm uniform cross-section, was simply supported. It was made from a solid rectangular mild steel bar with a density of 7335 kg/m^3 and a flexural stiffness $EI = 29{\cdot}97\mathrm{kN/m^2}$. The first three theoretical natural frequencies of the main beam bridge were calculated as $f_1 = 4{\cdot}5$ Hz, $f_2 = 18{\cdot}6$ Hz, and $f_3 = 40{\cdot}5$ Hz.

A U-shape aluminum track was glued to the upper surface of the main beam as a guide way for the model car, which was pulled along by a string wound the drive wheel of an electric motor. The speed of the motor could be adjusted. Seven photoelectric sensors were mounted on the beams to measure and check the uniformity of moving speed of the model car. Seven equally spaced strain gauges and three equally spaced accelerometers were mounted on the lower surface of the main beam to measure the response. A system calibration of the strain gauges was carried out before the actual testing program by adding

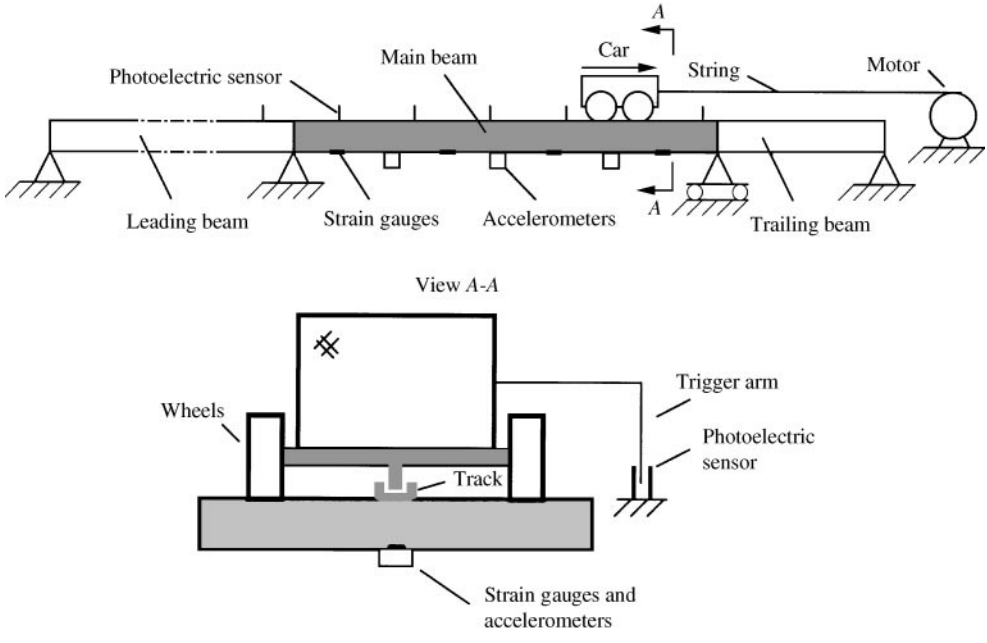

Figure 3. Experimental set-up of moving force identification.

masses at the middle of the main beam. A 14-channel tape recorder was employed to record the response signals. The first seven channels were used for logging the bending moment response signals from the strain gauges. Channels 8–10 were used for logging the accelerations from the accelerometers. Channel 11 was connected to the photoelectric sensors. In addition, the response signals from channels 1–7 and 11 were also recorded simultaneously on a PC for easy analysis. The software Global Lab from the Data Translation was used for data acquisition and analysis in the laboratory test. Before exporting the measured data in ASCII format for identification, the Bessel IIR digital filter with low-pass characteristics was implemented as cascaded second order systems. The Nyquist fraction value was chosen to be 0·03.

4. COMPARATIVE STUDIES ON THE FOUR IDENTIFICATION METHODS

Many parameters play an important role in the identification of moving forces. This comparative study is to investigate the effects of several main parameters on the all these four identification methods. The parameters studied include the sampling frequency, the mode number used, the speed of the vehicle, the computational time, the measuring sensor numbers and sensor locations. For practical reasons, the parameters were studied one at a time. The procedure was to examine each parameter in studied cases and to isolate the case with the highest accuracy for the corresponding parameter. There are two ways to check the accuracy. One is to check the identified results *directly* by comparing the identified forces with the true forces. However, as the true forces are unknown, this is not practical. The other way is to check the identified results *indirectly* by comparing the measured responses such as bending moments, displacements or accelerations with the rebuilt ones calculated from the identified forces. The accuracy is quantitatively defined as

equation (20), called a relative percentage error (RPE),

$$\text{RPE} = \frac{\sum |f_{true} - f_{ident}|}{\sum |f_{true}|} \times 100\%. \tag{20}$$

Equation (20) is also used to calculate the relative percentage errors between the measured and rebuilt responses instead of comparing the identified forces with the true forces directly. The measured response ($R_{measured}$) and rebuilt response ($R_{rebuilt}$) are substituted for the true force (f_{true}) and identified force (f_{ident}) in equation (20) respectively. In the present comparative studies, the results were based on the measurements of bending moments. The maximum acceptable RPE value adopted is 10%. The results associated with the accelerations will be reported separately.

4.1. EFFECT OF SAMPLING FREQUENCY

In the laboratory experiment, the data were acquired at a sampling frequency of 1000 Hz per channel for all cases. This sampling frequency was higher than the practical demand because only a few first lower frequency modes are usually used in moving force identification [11]. Therefore, the sequential data acquired at 1000 Hz was sampled again at a few intervals in order to obtain new sequential data at a lower sampling frequency. New sequential data at the sampling frequencies of 333, 250, and 200 Hz would be obtained by sampling the data again at every third, fourth and fifth point respectively. For each method, the identified forces were first calculated based on the bending moment response from all seven measuring stations. The rebuilt responses were then computed accordingly from the identified forces, the RPE values between the rebuilt and measured bending moment responses at each station were finally tested for validation of each identification method.

In the TDM and FTDM studies, the sampling frequency f_s should be high enough to ensure sufficient accuracy in the discrete integration in both equations (14) and (15) [11]. As there is a computer memory problem in the computation of the inverse of a large matrix in equation (18), the maximum sampling frequency is limited to be within 500 Hz, the sampling frequencies of 200, 250 and 333 Hz were set here. For the IMI and IMII, there is no memory problem, and the sampling frequencies of 200, 250, 333, 400, 500 and 1000 Hz were tested. The sampling frequency giving the highest accuracy will be adopted for the subsequent study of the effect of other parameters, i.e., the mode number (MN) used, the speed of the vehicle, the sensor numbers and the sensor locations.

Cases with three different car speeds, 5, 10, and 15 Units (1 Unit $\cong$ 0·102 m/s) were studied. Figure 4 plots typical effects of the sampling frequency on the four identification methods. Obviously, the effect of sampling frequency using the IMI and IMII is not so significant within 333 Hz, but it is significant if the sampling frequency is equal to and larger than 500 Hz. The RPE values grew to be the highest at the sampling frequency $f_s = 1000$ Hz. The corresponding RPE curve is not shown here as the RPE values at all seven stations are larger than 10% and can be as large as 18·93% for the IMI and 26·86% for the IMII. For the FTDM, the effect on identification accuracy increases with increase in the sampling frequency. The FTDM is not effective as the sampling frequency increases up to 333 Hz and the result is not incorporated in Figure 4 due to too high the RPE value. This shows that the IMI, IMII and FTDM are suitable for a lower sampling frequency, the highest accuracy is corresponding to the case of the lowest sampling frequency of $f_s = 200$ Hz. The effect of sampling frequency using the TDM is completely different from the above three methods. The higher the sampling frequency, the lower are the RPE values

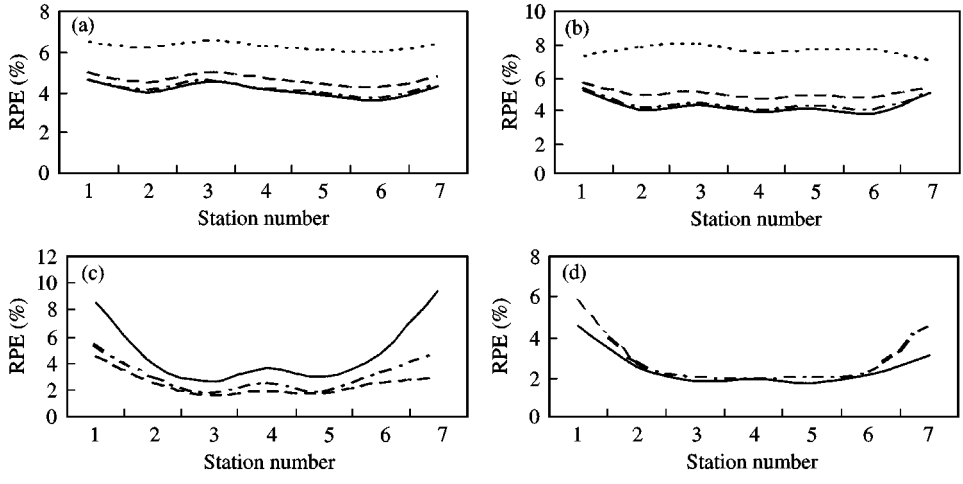

Figure 4. Effect of sampling frequency. —— 200 Hz; – · – · – 250 Hz; – – – 333 Hz; - - - - 500 Hz. (a) IMI (10 units); (b) IMII (10 units, MN = 3); (c) TDM (15 units, MN = 5); (d) FTDM (15 units, MN = 5).

for all the measuring stations. The TDM is suitable for the higher sampling frequency, the highest identification accuracy corresponds to the highest sampling frequency $f_s = 333$ Hz. Figure 4 also shows that both the TDM and FTDM give higher identification accuracy than either the IMI or IMII, especially at the middle measuring stations.

4.2. EFFECT OF MODE NUMBER USED (MN)

The IMI is independent of the mode number and the effect of mode number used on the IMI is not incorporated in this section. To compare the effects of different mode number on identified results, it was assumed that the sampling frequency (f_s) and vehicle speed (c) were not changed, and the mode number was changed one at a time. The bending moment data at all seven measurement stations were used to identify the moving forces.

Table 1 shows the results of RPE for the IMII with $c = 10$ Units, $f_s = 333{\cdot}333$ Hz. It shows that the IMII is unable to identify the two moving forces when the mode number is less than or equal to 2. However, if the mode number is greater than 2, the identification accuracy is acceptable but it decreases gradually with increase in the mode number. The best case is for MN = 3, or 4 in all the study cases, demonstrating that the IMII needs at least the first three modes or above to effectively identify the two moving forces with acceptable accuracy.

For both the TDM and FTDM, the case of $f_s = 250$ Hz, $c = 15$ Units was chosen. The mode number was varied from MN = 3 to MN = 10. The RPE values of the TDM and FTDM are given in Tables 2 and 3 respectively. If the mode number is less than or equal to 3, the tables show that the RPE results are not acceptable and both the TDM and FTDM failed to identify the two moving forces. However, if the mode number is larger than 3, the relative percentage errors reduce dramatically. Further, for the TDM, the RPE values increase gradually with an increase in the model number. If the mode number increases up to MN = 10, the TDM is again not effective at all measuring stations except station 4. For the FTDM, the RPE values decrease slightly with an increase in the mode number. This shows that these two methods are also effective if the required mode number is achieved or exceeded but otherwise fail. It is also found that the RPE values at the middle measuring

TABLE 1

Effect of mode number (MN) on IMII (10 Units, 333 Hz)

	RPE (%)						
MN	*sta.* 1	*sta.* 2	*sta.* 3	*sta.* 4	*sta.* 5	*sta.* 6	*sta.* 7
1	22·18	15·25	13·82	11·57	13·18	17·40	29·12
2	94·91	57·80	54·02	55·24	56·97	63·63	97·00
3	5·84	5·08	5·32	4·92	5·08	4·95	5·67
4	6·19	5·07	5·34	4·91	5·01	4·82	5·97
5	7·47	6·61	6·74	6·12	5·94	5·92	6·89
6	8·37	7·51	7·57	7·23	7·14	7·17	7·78

Shaded figures show the RPE > 10%.

TABLE 2

Effect of mode number (MN) on TDM (15 Units, 250 Hz)

	RPE (%)						
MN	*sta.* 1	*sta.* 2	*sta.* 3	*sta.* 4	*sta.* 5	*sta.* 6	*sta.* 7
3	305·67	199·10	103·41	113·08	101·44	192·07	282·38
4	5·80	3·32	1·89	2·86	1·98	3·77	5·75
5	5·42	3·08	1·80	2·58	1·95	3·44	4·83
6	8·09	3·78	2·57	2·43	2·75	4·66	7·12
7	14·27	6·45	6·89	3·95	6·58	5·38	10·96
8	14·27	6·45	6·89	3·95	6·58	5·38	10·96
9	14·28	6·48	6·88	3·96	6·56	5·39	10·94
10	21·24	13·83	10·11	5·01	10·01	13·11	19·37

TABLE 3

Effect of mode number (MN) on FTDM (15 Units, 250 Hz)

	RPE (%)						
MN	*sta.* 1	*sta.* 2	*sta.* 3	*sta.* 4	*sta.* 5	*sta.* 6	*sta.* 7
3	1602·00	1641·89	1664·82	1643·41	1622·99	1572·60	1474·81
4	13·58	7·19	5·69	5·93	5·55	6·75	12·91
5	5·74	2·80	2·15	2·08	2·14	2·41	4·74
6	4·91	2·72	1·89	2·05	1·73	1·87	3·45
7	4·79	2·44	1·54	1·73	1·39	1·57	3·07
8	4·73	2·42	1·53	1·64	1·35	1·50	3·05
9	4·59	2·30	1·50	1·63	1·30	1·49	3·20
10	5·05	2·23	1·52	1·96	1·34	1·62	4·24

stations are always less than the ones at the two end measuring stations. This is associated with the signal-to-noise ratio of various measurement stations because there are higher signal-to-noise ratios at the middle stations than at the two end stations. For the TDM, the minimum RPE value case is when MN = 5 and the maximum RPE value case is at the

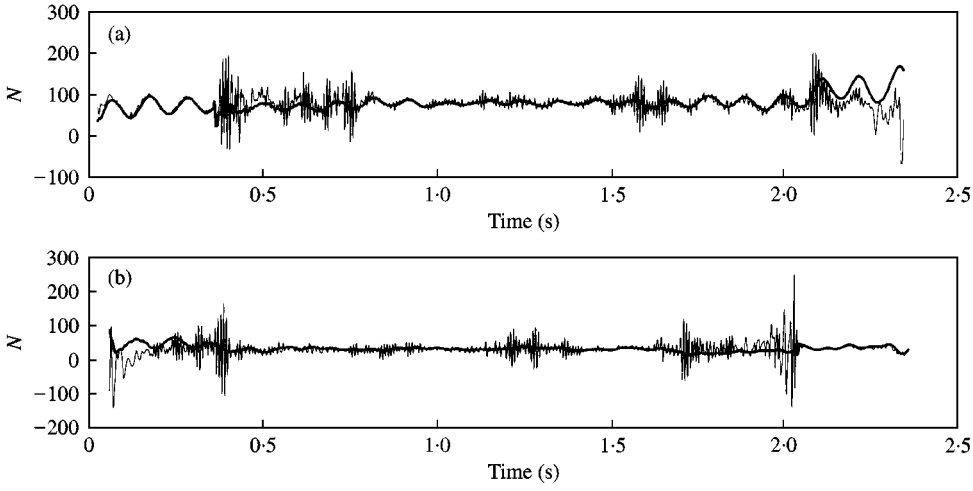

Figure 5. Identified forces in MN = 5, 250 Hz, 15 Units: (a) front axle; (b) rear axle. ▬ TDM, —— FTDM.

biggest mode number of 10. This shows that MN = 5 is the most accurate identification case in comparisons of this kind. However, the situation is not same as that for the FTDM. The biggest difference from the TDM is that the RPE value is almost independent of the mode number although there is a slight decrease of the RPE value after MN = 5.

Comparing the identification accuracy of the TDM and FTDM, it can be seen that the results are very close to each other when MN = 5, especially at the middle measuring stations. However, it can be seen from the identified forces in Figure 5 that the FTDM is apparently worse than the TDM because it has components with higher frequency noise.

4.3. EFFECTS OF VARIOUS VEHICLE SPEEDS

When the test was carried out, the three vehicle speeds were set manually at 5, 10 and 15 Units, respectively. After acquiring the data, the speed of the vehicle was calculated and the uniformity of the speed was checked. If the speed was stable, the experiment was repeated five times for each speed case to check whether or not the properties of the structure and the measurement system had changed. If no significant change was found, the corresponding recorded data was accepted for identification of the moving forces. After checking the speed of the vehicle between two triggers, it was found that apparent differences of the speed exist in each segment of the beam. Therefore,e the initial velocity and acceleration of the vehicle are used in the IMI and IMII. However, the average speed of the vehicle on the whole beam is used to identify the moving forces in the TDM and FTDM.

Table 4 shows the RPE values of all IMI study cases in which the sampling frequency is 250 Hz. There are five sets of recorded data for each speed case. Case 5-1 means the *first set* of data was recorded while the vehicle moves across the bridge at the speed of 5-Units. Others are similarly identified. It can be seen that there are five cases with unacceptable RPE values higher than 10%. These are Cases 5-1, 10-2, 15-1, 15-4, and 15-5 in which Case 15-5 is the worst. The most accurate cases are Cases 5-2, 10-4 and 15-3 by comparing each speed set. Figure 6 shows identified force results from the best case, Case 10-4 and the worst case, Case 10-2 for 10 Units set of speeds. Obviously, the magnitude of the scatter around the static wheel axle force in Case 10-2 is bigger than that for Case 10-4, both when

TABLE 4

Effect of vehicle speed on IMI

	RPE (%)						
Case	*sta.* 1	*sta.* 2	*sta.* 3	*sta.* 4	*sta.* 5	*sta.* 6	*sta.* 7
5–1	13·78	12·90	14·89	17·24	13·61	10·71	9·85
5–2	5·25	5·64	6·16	6·63	7·23	7·47	6·69
5–3	7·75	8·51	8·81	8·90	8·58	8·13	7·67
5–4	7·16	7·58	8·38	8·04	7·88	7·16	6·78
5–5	5·50	6·20	6·68	6·54	6·54	6·13	5·49
10–1	8·00	8·79	9·15	9·08	8·91	8·70	7·83
10–2	9·82	10·18	11·14	11·81	12·83	13·10	12·44
10–3	4·88	5·28	5·46	5·40	5·80	5·79	5·34
10–4	4·76	4·23	4·73	4·34	4·10	3·87	4·54
10–5	4·83	5·49	6·18	6·19	6·58	6·27	5·46
15–1	10·68	10·87	11·19	10·76	10·65	10·31	9·52
15–2	9·37	9·51	9·73	9·62	9·55	9·14	8·36
15–3	6·96	5·77	5·64	5·04	4·71	4·30	3·96
15–4	15·48	15·69	15·93	15·32	14·51	13·46	11·96
15–5	28·34	29·23	29·85	29·29	29·14	28·24	26·30

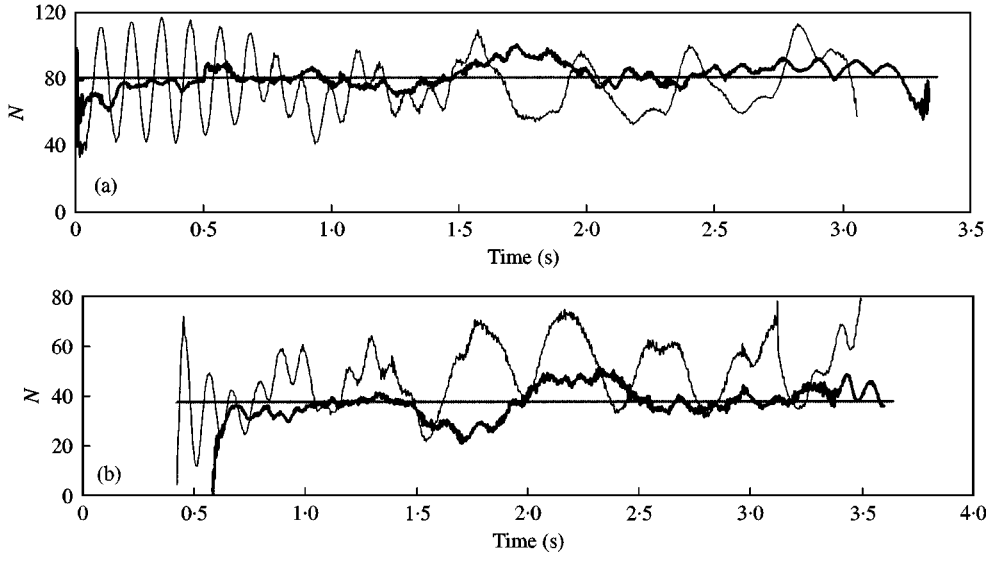

Figure 6. Identified by IMI in 250 Hz: (a) front axle, (b) rear axle, (▬ 10–4; —— 10–2; ▬ static).

comparing the front wheel forces identified and the rear wheel forces. This shows that the identified forces in Case 10-4 are more accurate than those in Case 10-2. Of course, the rebuilt response from the more accurate forces identified also show higher accuracy. Comparing all the RPE values at different speed sets, the lowest RPE level relates to 10 Units, and there are more acceptable results in the lower speed cases of 5 and 10 Units than in the cases of 15 Units.

TABLE 5

Effect of vehicle speed on IMII($MN = 3$, 250 *Hz*)

	RPE (%)						
Case	*sta.* 1	*sta.* 2	*sta.* 3	*sta.* 4	*sta.* 5	*sta.* 6	*sta.* 7
5–1	15·73	11·50	13·95	7·15	13·52	9·35	15·87
5–2	11·64	7·47	8·70	6·18	7·61	7·28	12·85
5–3	15·06	11·07	11·93	10·67	11·12	10·08	15·22
5–4	14·39	10·32	11·44	9·46	10·25	9·49	14·62
5–5	12·36	8·56	9·87	7·81	8·66	7·68	13·47
10–1	12·03	6·62	7·56	6·67	7·00	5·83	13·82
10–2	14·41	10·54	11·31	10·23	11·00	10·06	13·61
10–3	12·71	8·67	9·37	7·38	8·46	7·60	13·13
10–4	12·90	6·89	8·45	6·63	7·71	6·76	13·18
10–5	13·56	10·00	10·91	8·79	10·03	8·93	13·47
15–1	12·31	6·63	7·11	4·55	5·93	5·66	13·02
15–2	12·23	6·00	6·98	4·40	6·05	5·75	13·21
15–3	13·75	8·46	9·45	7·08	7·90	7·69	13·61
15–4	13·88	7·57	8·79	6·70	7·50	6·31	13·75
15–5	15·05	8·51	8·72	6·47	7·81	7·38	14·25

Table 5 shows the RPE value for all IMII study cases. In each case, the mode number MN = 3, and the sampling frequency $f_s = 250$ Hz. The results show that the RPE values at stations 1 and 7 are bigger than 10% in all cases, the RPE values are also bigger than 10% in Cases 5-1, 5-3, 5-4, 10-2, 10-5. Therefore, they are all unacceptable due to worse identification accuracy. After comparing the results at three sets of different vehicle speeds, it is found that the 15 Units speed set has a better result except at the stations 1 and 7. This shows that the IMII is more suitable for the identification with a higher vehicle speed.

Each identification method was implemented using the programming language FORTRAN 90. The program consists of two parts. One is force identification from the measured responses and the other a calculation of rebuilt responses from the forces identified. In the IMII study, if the moving forces are identified by the IMII, the rebuilt bending moment response will be calculated by the IMI but not the IMII, and the RPE results are found to be similar to Table 4 by the IMI. It can be seen that the accuracy of rebuilt responses at the 5 Units set is higher than those in Table 5, but the accuracy at 15 Units is completely opposite. All of these show that the IMI is applicable for the set of the lower 5 and 10 Unit speeds, but the IMII is applicable for the set of the higher 15 Units speed. Figure 7 shows the comparison of effect of the speed on the IMI and IMII through the rebuilt responses at the same station 4. At the 15 Units, the IMII rebuilt responses are in better agreement with the measured one than that for the IMI. However, at the 5 Units, the IMI rebuilt responses are in better agreement with the measured one although these rebuilt responses have a lot of noise.

In this section, some limitations on the TDM and FTDM have been considered firstly. In particular, necessary RAM memory and CPU speed of personal computer are required for both the TDM and FTDM. Otherwise, they will take a significant amount of execution time due to large size of the system coefficient matrix **B** in equation (18), or they cannot be executed at all due to insufficient memory. If the mode number, the sampling frequency and bridge span length had not been changed for this case, a change of the vehicle speed would

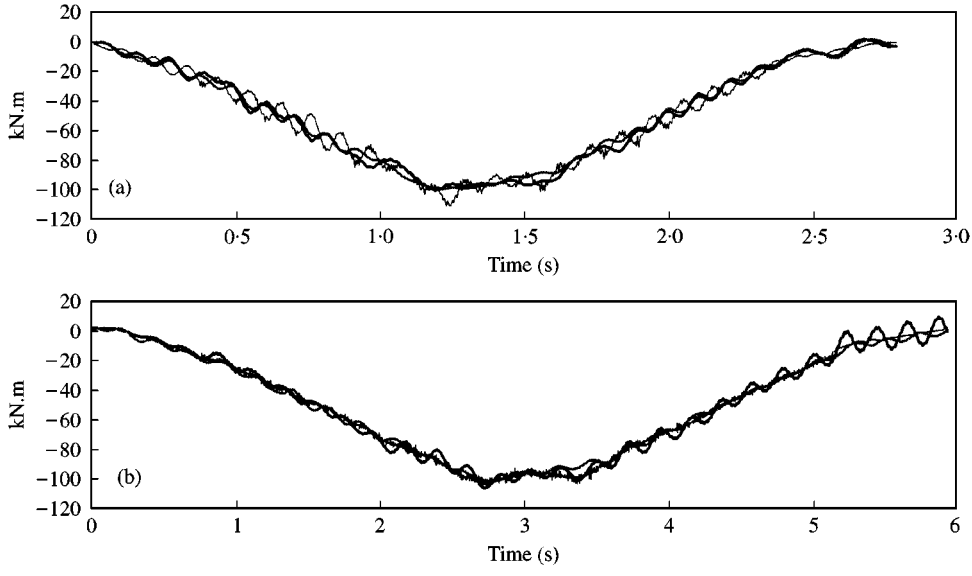

Figure 7. Comparison of Responses at Station 4 in 250 Hz; (a) at 15 Units, (b) at 5 Units, (—— IMI; ▬▬ IMII; ▬▬ Measured).

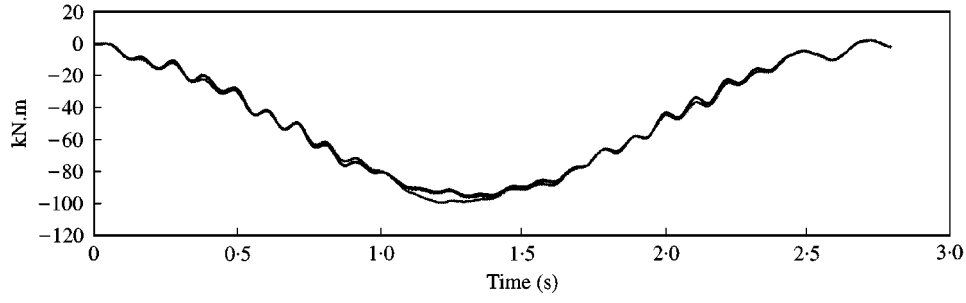

Figure 8. Comparison of Responses at Station 4 in MN = 4, 200 Hz (—— TDM; ▬▬ FTDM; ▬▬ Measured).

mean a change of the sampling point number, which will in turn change the dimensions of matrix **B** in equation (18). Therefore, in order to make the TDM and FTDM effective and to analyze the effects of various vehicle speeds on the identified results, the case with MN = 4, f_s = 200 Hz was selected. The RPE values are calculated and tabulated in Table 6 for Cases 5-2, 10-4 and 15-2. It shows that the TDM is effective for all three various vehicle speeds. Although the change in the RPE value is not so significant, the RPE values tend to be reduced especially for those at the middle measuring stations while the vehicle speed increases. However, the FTDM failed to identify the forces while the vehicle speed is lower, say 5 Units, but the identified results are getting better and better as the vehicle speed increases. Fortunately, the identified result is acceptable at last in the case of 15 Units for the FTDM. These results show that the identification accuracy for the faster vehicle speed is higher than that at lower vehicle speed for both the TDM and FTDM. Figure 8 shows a comparison of rebuilt responses at station 4 by the TDM and FTDM. The rebuilt responses of the TDM and FTDM agree well with the measured ones except some points between 1·1 and 1·4 s.

TABLE 6

Effect of vehicle speed on TDM and FTDM ($MN = 4, f_s = 200$ Hz)

	RPE (%)					
	TDM			*FTDM*		
Station no.	5-2	10-4	15-2	5-2	10-4	15-2
1	5·23	5·89	6·71	5350·8	110·01	5·94
2	3·48	2·66	3·30	2807·2	50·02	3·29
3	2·88	2·95	2·42	2251·5	25·87	2·05
4	3·31	3·20	3·01	1940.4	48·23	2·66
5	2·80	2·76	2·58	2171·8	24·75	2·01
6	4·22	3·91	3·96	2732·4	47·60	3·57
7	5·78	7·38	6·29	5173·6	101·65	5·89

4.4. EFFECT OF VARIOUS SENSOR NUMBERS

Chan and O'Connor [15] have proposed two formulae for determination of the required number of strain gauges for the IMI. Chan *et al.* [13] also defined a formula to recommend the number of sensors for the IMII. Therefore, the effects of sensor on the IMI and IMII will not be taken into consideration here. For the TDM and FTDM, the sensor number N_l was set to 2, 3, 4, 5, and 7 respectively, while the other parameters MN = 5, $f_s = 250$ Hz, $c = 15$ Units were not changed for all study cases. The RPE values are given in Table 7. It shows that the TDM requires at least three, best have four measurement stations to obtain the two correct moving forces. However, the FTDM should have at least one more measurement station than using the TDM, i.e., 4, to obtain the same number of moving forces. However, the RPE errors are increased obviously when the measurement station number is equal to 5 for the FTDM. This is because the addition of the fifth station is placed on the $1/2L$ point, namely the node of the second and fourth modes of the supported beam. Nevertheless, when $N_l = 7$, i.e., put two more stations at the $1/8L$ and $7/8L$ respectively, the RPE values by the FTDM recover normal level to within 10%. It indicates that the FTDM is sensitive to the locations of measuring station, and they should be selected carefully. In general, for the TDM and FTDM, the identification accuracy is better if more measuring stations are adopted, but it will take longer computational time.

4.5. COMPARISON OF COMPUTATIONAL TIME

As the computation process of both the IMI and IMII takes only a few minutes in any study case, it is not significant in a measurement of the computational time. However, there exists a different situation for the TDM and the FTDM, in which the computational time consists of three parts, i.e., (i) forming the system coefficient matrix **B** in equation (18), (ii) identifying forces by solving equation (18) and (iii) producing the rebuilt responses. The above parts are the same for the TDM and FTDM. The case described here is of MN = 5, $f_s = 250$ Hz, $c = 15$ Units, $N_l = 7$ by using a Pentium II 266 MHz CPU, 64 M RAM computer. The total sampling points for bending moment response at each measuring station are 700 and the total sampling points for each wheel axle force are 604 in the time domain. Therefore, the dimensions of matrix **B** are $(7 \times 700, 2 \times 604)$. A detailed comparison of the execution time for each part of the TDM and FTDM is recorded in Table 8. It shows

TABLE 7

Effect of measuring station number on TDM and FTDM

	RPE (%)									
	TDM					*FTDM*				
	$N_l = 2$	$N_l = 3$	$N_l = 4$	$N_l = 5$	$N_l = 7$	$N_l = 2$	$N_l = 3$	$N_l = 4$	$N_l = 5$	$N_l = 7$
Sta. 1	*	*	*	*	5·42	*	*	*	*	5·74
Sta. 2	*	*	1·48	2·17	3·08	*	*	2·90	34·63	2·80
Sta. 3	1815	15·76	1·44	1·80	1·80	1160	70·15	2·09	17·25	2·15
Sta. 4	*	13·39	*	2·67	2·58	*	77·27	*	34·68	2·08
Sta. 5	1788	8·33	1·85	1·94	1·95	1138	73·90	2·11	16·65	2·14
Sta. 6	*	*	1·56	1·98	3·44	*	*	2·74	32·87	2·41
Sta. 7	*	*	*	*	4·83	*	*	*	*	4·74

Asterisk * indicates the station is not chosen.

TABLE 8

Comparison of computational time (*in s*)

PART	TDM	FTDM
Forming coefficient matrix B	332·69	1059·57
Identifying forces	1837·97	1834·07
Rebuilding responses	55·04	53·99
Total	2225·7	2947·63

that the FTDM takes much longer than the TDM to form the coefficient matrix **B**. The execution time in the (ii) and (iii) parts is almost the same for the two methods. Thus, the total execution time is shorter for the TDM than that for the FTDM.

5. CONCLUSIONS

In this paper, it can be seen that it is successful to use the bridge strain responses to accurately identify the axle force history of a moving vehicle on bridges. Comparative studies on moving force identification have been carried out in the laboratory. The effects of parameters, such as the sampling frequencies, the mode numbers, the vehicle speeds, the computational time, the sensor numbers and locations, have been investigated. The following conclusions are drawn. (1) The effects of sampling frequency using the IMI and IMII are not too obvious within 333 Hz range, but after this range, the effects become more significant, especially for $f_s = 1000$ Hz, both the IMI and IMII fail. For the FTDM, the effect of sampling frequency increases with the sampling frequency, and the FTDM fails if the higher sampling frequency 333 Hz is adopted. However, the TDM is suitable for the higher sampling frequency, it has the highest identification accuracy when the highest sampling frequency 333 Hz is employed. Moreover, both the TDM and FTDM have higher identification accuracy than both the IMI and IMII. (2) The IMI is independent of the mode number. The IMII needs at least the first three modes or more to correctly identify the two

moving forces. For both the TDM and FTDM, the minimal necessary mode number required is 4. If the first five modes are used to identify the two moving forces, the identification accuracy is the highest in the cases studied. Further, from the point of view of the identified forces, the TDM is better than the FTDM. (3) For the IMI, there are more acceptable results in the lower speed cases of 5 and 10 Units than in the cases of 15 Units. However, the IMII is more suitable for the higher vehicle speed. The faster vehicle speed is also of benefit to both the TDM and FTDM. The TDM can effectively identify the forces in all the speed cases, but the FTDM fails in the lower speed cases of 5 and 10 Units. (4) At least three and four measuring stations are recommended to identify the two wheel-axle forces using the TDM and FTDM respectively. The locations of the measuring stations should be carefully selected, especially for the FTDM. (5) The TDM takes a shorter execution time than the FTDM. (6) All four identification methods can effectively identify moving forces, and can be accepted as practical methods with higher identification accuracy. (7) From the point of view of all the parameter effects on the identification accuracy, the TDM is the best identification method except for the executive time.

All the above findings are important for the further development of the moving force identification system (MFIS) to acquire real data in the field. To conclude, as a feasible method, the TDM should be firstly recommended as a practical method to be incorporated into the MFIS.

ACKNOWLEDGMENT

The present project was supported by the Hong Kong Reseach Grants Council.

REFERENCES

1. O. K. NORMANN and C. R. HOPKINS 1952 *Weighing vehicles in motion. Highway Research Board Bulletin* 50, National Research Council, Washington, DC.
2. L. FRYBA 1972 *Vibration of Solids and Structure under Moving Loads.* Prague: Noordhoff International Publishing.
3. B. TRITT and B. RICHARDS 1978 *Proceeding of Axle Mass Determination Workshop ARRB, Australia.* Determination of vehicle axle mass: a description and demonstration of the ARRB system.
4. F. MOSES 1984 *Journal of Transportation Engineering ASCE* **105**, 233–249. Weigh-in-motion system using instrumented bridge.
5. R. J. PETERS 1984 *Proceeding of 12th ARRB Conference, Hobart, Australia*, Vol. 2, 10–18. AXWAY–a system to obtain vehicle axle weight.
6. R. T. PETERS 1986 *Proceedings of 13th ARRB and 5th REAAA Combined Conference, Australia*, Vol. 6, 70–83. CULWAY—an unmanned and undetectable highway speed vehicle weighting system.
7. M. HOSHIYA and O. MARUYAMA 1987 *Journal of Engineering Mechanics ASCE*, **113**, 813–824. Identification of running load and beam system.
8. J. C. BRIGGS and M. K. TSE 1992 *International Journal of Impact Engineering* **12**, 361–372. Impact force identification using extracted modal parameters and pattern matching.
9. K. K. STEVENS 1987 *Proceedings of SEM Spring Conference on Experimental Mechanics, FL, USA* 838–844. Force identification problems—an overview.
10. C. O'CONNOR and T. H. T. CHAN 1988 *Journal of Structural Engineering ASCE*, **114**, 1703–1723. Dynamic wheel loads from bridge strains.
11. S. S. LAW, T. H. T. CHAN and Q. H. ZENG 1997 *Journal of Sound and Vibration*, **201**, 1–22. Moving force identification: a time domain method.
12. S. S. LAW, T. H. T. CHAN and Q. H. ZENG 1999 *Journal of Dynamic System, Measurement and Control* **121**, 394–401. Moving force identification—a frequency and time domains analysis.

13. T. H. T. CHAN, S. S. LAW, T. H. YUNG and X. R. YUAN 1999 *Journal of Sound and Vibration* **219**, 503–524. An interpretive method for moving force identification.
14. T. H. YUNG 1999 *Ph.D. Thesis*, Hong Kong Polytechnic University, Hong Kong: Assessment of highway loading from bridge responses.
15. T. H. T. CHAN and C. O'CONNOR 1990 *Journal of Structural Engineering ASCE* **116**, 1751–1771. Wheel loads from highway bridge strains: field studies.